The Aeronautical Journal (2022), **126**, pp. 889–905
doi:10.1017/aer.2021.118

REGULAR PAPER

Sensor fault detection and reconstruction system for commercial aircrafts

U. Kilic[1,*] and G. Unal[2]

[1]Department of Avionics, Erzincan Binali Yildirim University, Erzincan, 24002, Turkey and [2]Department of Avionics, Eskisehir Technical University, Eskisehir, 26470, Turkey
*Corresponding author. Email: ugur.kilic@erzincan.edu.tr

Received: 27 June 2021; **Revised:** 12 October 2021; **Accepted:** 25 November 2021

Keywords: Aircraft sensor; Fault detection; Reconstruction; Machine learning

Abstract

The aim morphing of this study is to detect and reconstruct a fault in angle-of-attack sensor and pitot probes that are components in commercial aircrafts, without false alarm and no need for additional measurements. Real flight data collected from a local airline was used to design the relevant system. Correlation analysis was performed to select the data related to the angle-of-attack and airspeed. Fault detection and reconstruction were carried out by using Adaptive Neural Fuzzy Inference System (ANFIS) and Artificial Neural Networks (ANN), which are machine-learning methods. No false alarm was detected when the fault test following the fault modeling was carried out at 0–1 s range by filtering the residual signal. When the fault was detected, fault reconstruction process was initiated so that system output could be achieved according to estimated sensor data. Instead of using the methods based on hardware redundancy, we designed a new system within the scope of this study.

Nomenclature

E	expected value
g	gravitational acceleration (m/s^2)
i	boole variable
j	subscript index
k	index
n	total data
p	correlation coefficient
R	gas constant (J/kgK)
t	time (s)
T_0	sea-level temperature (K)
X	input data
Y	output data
α_c	consolidated angle-of-attack data (deg)
$\bar{\alpha}$	the vector involving left, right and back-up angle-of-attack measurement signal (deg)
α_k	the angle-of-attack data (deg)
ε_1	threshold value for the unfiltered residual signal
ε_2	threshold value for the filtered residual signal
μ	mean value
ρ_0	sea-level density value (kg/m^3)
ρ	the density value (kg/m^3)
σ	standard deviation
φ	relative density value

© The Author(s), 2021. Published by Cambridge University Press on behalf of Royal Aeronautical Society.

https://doi.org/10.1017/aer.2021.118 Published online by Cambridge University Press

1.0 Introduction

While accidents on the aircrafts can be reduced with the training to be given to the flight crew, the elimination of the faults on the aircraft requires engineering work. Therefore, the starting point of this study was the question of what can be done to eliminate these faults. Accidents have occurred due to angle-of-attack and airspeed sensors. A Boeing 737 Max aircraft belonging to Lion airlines crashed in the Java Sea due to an angle-of-attack sensor failure on October 29, 2018. A Boeing 737 Max aircraft belonging to Ethiopian Airlines crashed near the town of Bishoftu also as a result of an angle-of-attack sensor failure on March 10, 2019. An Airbus A330 aircraft belonging to Air France crashed in the Atlantic Ocean due to pitot probes icing on June 1, 2009. It was reported that pitot probes were clogged by ice crystals during the cruise. An Airbus A330 aircraft belonging to Etihad Airways crashed in Australia on November 13, 2013. It was reported that pitot probes were clogged by mud dauber nest. An Antonov An-148 belonging to Saratov Airlines crashed in the Moscow due to pitot probes icing on February 11, 2018 [1].

Commercial aircraft manufacturers such as Boeing and Airbus generally add at least one sensor for angle-of-attack and at least two sensors for airspeed as backups. However, no matter how many redundant components are used for each sensor, all of the sensors will show incorrect data in case of any icing. Fault detection and reconstruction systems used for modern aircrafts in the literature are methods such as majority voting and weighted mean based on the majority accuracy of the primary/redundant sensors on the aircrafts. As shown in Eq. (1), output is computed by using weighted average method when fault-free condition. As shown in Eq. (2), in case of fault, if the sensor data variation of a sensor is more than that of other two, the average of other two sensors is transferred to the output. However, if the two sensor data are incorrect, in this case, the incorrect sensor data is transferred to the output [2]. The best example here is the Air France Flight 447 accident on June 1, 2009. In the triple redundant pitot probe system, two probes are frozen, so the average of the erroneous data is transferred to the output.

$$\alpha_c = \frac{1}{2} median\,(\bar{\alpha}) + \frac{1}{4}\,(min\,(\bar{\alpha}) + max\,(\bar{\alpha})) \tag{1}$$

$$\alpha_c = \frac{1}{2}\sum\nolimits_{k=1}^{3} \alpha_k i_k \tag{2}$$

Therefore, instead of adding a new sensor, it would be more advantageous to detect and reconstruct the fault according to the estimated sensor data. In this way, flight crew will be prevented from flying according to faulty data. In addition, weight and production/maintenance costs can be saved by reducing hardware redundancy. The point to note here is that the data used for the reconstruction of faulty values are not obtained from any redundant element and are estimated from other data. The real flight data collected from a local airline was used for the system design. Firstly, data related to the angle-of-attack and airspeed were selected by correlation analysis. Based on the related data, the required values of the angle-of-attack and airspeed data were estimated. Machine learning methods are widely used in recent studies for modeling and estimation especially in the aerospace fields [3–9]. In this study, machine learning based methods which are Adaptive Neural Fuzzy Inference System (ANFIS) and Artificial Neural Networks (ANN) were used in the estimation phase [38]. MATLAB software was used for all the calculations.

Angle-of-attack sensors are very important components because they drive systems such as stall warning, stall margin information on airspeed indicators, and pitch limit indicator (PLI). For direct measurement of the angle-of-attack generally pivoted vanes or pressure type sensors are used in the literature. Pivoted vane sensors are placed either on the common boom with receivers of the total and static pressure or could also be mounted in the selected locations, but these type of sensors have some disadvantages due to its structure that changes with flight. However, pressure type sensors have different measurement method and this sensors operate based on measuring differential pressure on the flowed body using the air pressure with two pairs of holes placed symmetrically in relation to the central hole [10]. It is indicated that the improvement of angle-of-attack systems is useful for the stall prevention. It is examined that an alternative measurement method for pressure type sensors resulting the increasing

https://doi.org/10.1017/aer.2021.118 Published online by Cambridge University Press

number of the sensors would increase the accuracy of the estimation [11]. In addition, the angle-of-attack sensor faults were examined and the accuracy of this sensors are tried to increase in some studies [12,13]. Faults that may occur in the pitot-static system affect the airspeed, vertical speed and altitude data. There are two angle-of-attack sensors on commercial aircrafts (one captain-side angle-of-attack sensor, one F/O-side angle-of-attack sensor). Likewise, there are three pitot probes on commercial aircrafts (one captain-side pitot probe, one F/O-side pitot probe and one stand-by pitot probe). In addition, there are four Air Data Modules (ADM) that convert the air data received from the ports into numerical values and send them to the Air Data Inertial Reference Unit (ADIRU) [14]. The different manufacturers such as Aerosonic, AeroControllex, Collins Aerospace and Honeywell provide the relevant components for commercial aircrafts. There is no need for two ADM units with the removal of the one redundant angle-of-attack sensor and two redundant pitot probes in this study. By removing the redundant elements, an average of about 7 kg weight is saved on the aircraft. If the turbo fan CFM56 type engines using in commercial aircrafts are taken as an example, the thrust-specific fuel consumption (TSFC) of the relevant engines is approximately 0.667 kg/kg.hr (18.9 g/kN.s) [15]. In other words, the relevant aircrafts burn a total of 4.669 kg of fuel per hour for the redundant components. Considering that the relevant aircrafts fly 12 hours a day, approximately 20 tons of fuel is wasted annually due to redundant components [16]. In addition, with the reduction of fuel burned, an annual distance gain of 8,000 km was achieved for the aircraft (these aircrafts burn an average of 2.51 kg of fuel per km [17]). CO_2 emissions and fuel consumption in relevant aircrafts are associated with a 3.16 kg CO_2/kg jet fuel coefficient [18]. Since 20 tons of fuel could be saved in the study, approximately 63.2 tons less CO_2 emission was achieved annually.

The literature includes studies conducted based on the aircraft modeling [3,19–26]. However, studies based on the aircraft modeling have mostly been carried out for certain sensors and certain fault conditions during the cruise. In addition, these studies include certain assumptions, model uncertainties and measurement errors. If we explain some of the related studies; Zolghadri *et al.* (2015) examined the model and signal based fault detection methods for the aircraft electric flight control system (EFCS). The methods examined have been tested on a realistic aircraft model or with real flight data from an Airbus A380 aircraft [22]. Sercekman and Kutay (2018) proposed an innovative approach to an observer-based fault detection method. Fault detection was performed by evaluating the significant changes in the behaviour of the aircraft according to the predicted fault-free behaviour using the standard kalman filter as an observer [23]. Lijia *et al.* (2019) designed a fault detection system for the unmanned aerial vehicle location system by using the observer and radial-based functional network structure together [24]. He *et al.* (2020) created a model-based fault detection and diagnosis system by using the observer and kalman filter structure separately for the inertial measurement unit in aircraft. While the observer structure gives faster results in fault detection, fault detection can be carried out more precisely in the kalman filtered structure [25]. There are studies that do not detect faults, but are aimed at providing alternative data source based on real flight data using artificial neural networks [4,27]. In the first study, thrust data was tried to be calculated by using airspeed, altitude and temperature. In the second study, airspeed data was tried to be estimated without pitot-static system measurements. Among the studies carried out, there are studies in which all flight conditions (climb, cruise, descent) are taken for the fault detection and reconstruction based on real flight data [28,29]. However, these studies examine certain sensors and certain fault conditions (hard or soft bias). In addition, fault detection time delay and false alarms are encountered in these studies. If we mention about some practical work; Airbus A320, A330 and A340 are equipped with a Backup Speed Scale (BUSS), which is a theoretical airspeed is estimated from just pitch and thrust data; however, the system failed on Air France 447. Boeing attempted to solve this problem as equip the Boeing 787 with a virtual airspeed sensor calculated from angle-of-attack and inertial data which is named as Synthetic Air Speed (SAS); however, this system failed on Jetstar flight JQ 07. Although there are very important theoretical and practical studies, there is no generally used fault detection and reconstruction system in aircrafts. In this study, instead of a single fault type for angle-of-attack and airspeed sensors, different fault scenarios that can be encountered in all flight phases are examined. In addition, a more reliable fault detection and reconstruction system was created

https://doi.org/10.1017/aer.2021.118 Published online by Cambridge University Press

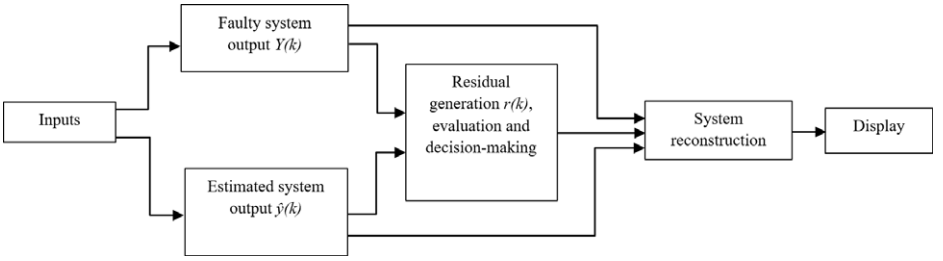

Figure 1. *Block diagram of the fault detection and reconstruction system.*

by eliminating the fault detection time delay and false alarm conditions that occurred in the related studies, and an alternative data source for angle-of-attack and airspeed was obtained for commercial aircrafts. Furthermore, instead of system like BUSS and SAS, the designed system contains more parameters for estimation. In this study, it is stated that the higher number of correlated input parameters result in better estimation phase as it is stated in further works of some studies.

2.0 Research methodology

2.1 General structure of the fault detection system

The fault detection phase consists of; residual generation (the difference between faulty data and estimated data), residual evaluation (according to a certain threshold value) and decision-making [30]. As it can be seen in Eq. (3), faulty system data *"Y(k)"* was formed by adding fault model *"f(k)"* at *"$t_1 \leq t \leq t_2$"* time interval on fault-free system data *"y(k)"*. Estimated system data *"$\hat{y}(k)$"* is independent of fault.

$$Y(k) = y(k) + f(k) \tag{3}$$

According to Eq. (4), residual value *"r(k)"* is equal to the difference between faulty system data *"Y(k)"* and estimated system data *"$\hat{y}(k)$"*.

$$r(k) = Y(k) - \hat{y}(k) \tag{4}$$

Threshold value being "ε'' as seen in Eq. (5), system will initiate fault detection when the absolute value of the residual exceeds the threshold.

$$|r(k)| > \varepsilon \tag{5}$$

The block diagram of the system designed for the fault detection and reconstruction is given in Fig. 1. When a fault is detected, it is intended to compensate the fault effects for safe operations. Thus, in order to increase the system performance, the faulty output measurements must be reconstructed. The estimated system data *"$\hat{y}(k)$"* provides the necessary information for this reconstruction. A simple fault reconstruction strategy is to replace the faulty output measurements *"Y(k)"* with the compensated measurements *"Y(k)-r(k)"* which means *"$\hat{y}(k)$"*. The accuracy of any fault detection system depends on detection time, false alarm rate and whether fault is detected or not [31].

In this study, we examined types of fault within the fault limits allowed by the authorities like FAA (Federal Aviation Administration). While the absolute value of the difference between the captain and F/O indicators for the angle-of-attack sensor should not exceed 10 degrees, for the airspeed sensor should not exceed 4 knots. It is stated that there is no fault condition up to these values, and they are acceptable. The angle-of-attack sensor output signal is affected by aerodynamic vibrations, which can oscillate the sensor data. Relevant sensors may contain bias faults due to magnetic environmental conditions [32]. One of the main reasons for these systems to fail is the clogging of the pitot-static system by ice or foreign objects. In the pitot probe, the total pressure inlet hole, the static pressure inlet hole or the drain hole can be clogged. If the total pressure inlet hole is clogged after the pitot tube drain hole is clogged,

https://doi.org/10.1017/aer.2021.118 Published online by Cambridge University Press

Table 1. *Some information about the flight data*

	Altitude (ft)	Airspeed (CAS) (knot)	Angle-of-attack (deg)	Vertical speed (ft/min)	Pitch angle (deg)	Total air temperature (degC)	N12 (rpm)
Mean	2.6474e+04	224.45	−1.2164	−4.1752	2.3991	−15.265	74.6664
Median	36,994	251	−0,88	0	2.8000	−19.500	89.6000
Standard deviation	1.4768e+04	76	2.1543	875.3582	1.9648	12.314	26.2614
Minimum	0	45	−18.46	−3344	−3	−38	19.1000
Maximum	37,048	327	9.14	4,272	17.4000	9.750	99.5000

and then the static pressure inlet hole on the pitot tube is clogged, the airspeed data will remain stuck at its last value. However, if the total pressure inlet hole is clogged first, then the airspeed indicator will go to zero and stuck. Examples include freezing water, insects that nest while the aircraft is parked, or the pitot tube and/or static hole covers not removed prior to flight. In addition, the water accumulated in the pitot-static system lines moves in the pipes with the effect of the acceleration force and changes the pressure of the trapped air, and it causes oscillation effect on the indicators [33].

2.2 Feature extraction and correlation analysis

Firstly, data related to angle-of-attack and airspeed data were selected by using correlation analysis. In other words, the features to be used in the system were selected with correlation analysis and the data was extracted. This makes it possible to process large data. Since the number of features are reduced, the training phase of the relevant algorithms takes less time. The accuracy is increased since the training data is cleared of unnecessary features. Some information about the flight data are given in Table 1.

Flight data used for the analysis; static pressure (hPa), altitude (ft), barometric altitude (ft), CAS (knot), TAS (knot), AOA (angle-of-attack, deg), vertical speed (ft/min), body rate roll (deg/s), body rate pitch (deg/s), body rate yaw (deg/s), roll angle (deg), pitch angle (deg), heading (deg), SAT (static air temp, degC), TAT (total air temp, degC), N11 (engine N1 shaft speed, rpm), N12 (engine N2 shaft speed, rpm). The airspeed is corrected as IAS (indicated airspeed) – CAS (calibrated airspeed) – EAS (equivalent airspeed) – TAS (true airspeed). As it can be seen in Eq. (6), TAS depends on the density value (ρ_0: air density at the sea level and ρ: air density at the related altitude, kg/m^3).

$$TAS = \frac{EAS}{\sqrt{\varphi}} \quad \left(\varphi = \frac{\rho}{\rho_0}\right) \tag{6}$$

Since there is a relation between density (ρ, kg/m^3) and altitude (h, m) data according to Eq. (7), TAS varies according to the altitude data [34]. Therefore, it would be more accurate to use CAS in calculations. As, $T_o = 288$ K, $g = 9.81$ m/s^2 and $R = 287$ J/kgK;

$$\frac{\rho}{\rho_0} = \left(1 - \frac{h}{44308}\right)^{4.259} \tag{7}$$

The correlation coefficient is a coefficient that indicates the direction and size of the relationship between independent variables. The related coefficient takes a value between −1 and +1, and the closer to −1 or +1, the more linearity of the relationship. This coefficient is obtained by dividing the covariance of the two examined variables by the product of the standard deviations of the variables. The correlation coefficient is calculated as given in Equation (8), and variables are taken without correlation when $|p| < 0.05$ in all practical applications [35].

$$p_{x,y} = \frac{Cov(X,\ Y)}{\sigma_x\, \sigma_y} = \frac{E(X - \mu_x)\left(Y - \mu_y\right)}{\sigma_x\, \sigma_y} \tag{8}$$

https://doi.org/10.1017/aer.2021.118 Published online by Cambridge University Press

Table 2. *Related data for angle-of-attack and correlation coefficients*

Related data for angle-of-attack	Static pressure (hPa)	CAS (knot)	Body rate pitch (deg/s)	Pitch angle (deg)	Heading (deg)	SAT (degC)	TAT (degC)	N11 (rpm)	N12 (rpm)
Corr. coeff.(*p)*	0.3128	0.5067	0.2252	0.5249	0.1956	0.2540	0.2241	0.3734	0.3723

Table 3. *Related data for airspeed and correlation coefficients*

Related data for airspeed	Static pressure (hPa)	Pitch angle (deg)	Heading (deg)	SAT (degC)	TAT (degC)	N11 (rpm)	N12 (rpm)
Corr. coeff.(*p)*	0.8342	0.4652	0.3731	0.8075	0.7455	0.7674	0.7656

In this study, firstly, the correlation analysis was carried out between the angle-of-attack data and other data and the absolute values of the correlation coefficients were obtained. Accordingly, the data related to the angle-of-attack as a result of the correlation analysis is a total of 12 (since $|p| < 0.05$, vertical speed, roll rate, yaw rate and roll angle have been eliminated). The altitude value is calculated according to the static pressure and the static pressure, altitude data and the altitude data read from the barometric altimeter are fed from the same source. Therefore, static pressure ($p = 0.3128$), which has the highest correlation between them, was included in the study. In addition, as mentioned before, CAS data was included in the study because TAS data changes with altitude. In this way, data related to the angle-of-attack and their correlation coefficients are given in Table 2.

Next, the correlation analysis was carried out between the airspeed data and other data, and the absolute values of the correlation coefficients were obtained. Accordingly, the data related to the airspeed as a result of the correlation analysis is a total of 10 (since $|p| < 0.05$, vertical speed, roll rate, pitch rate, yaw rate and roll angle have been eliminated). The altitude value is calculated according to the static pressure and the static pressure, altitude data and the altitude data read from the barometric altimeter are fed from the same source. Therefore, static pressure ($p = 0.8342$), which has the highest correlation between them, was included in the study. The calibration of the angle-of-attack data is carried out according to the Mach number, which is an airspeed data indication. In other words, the airspeed data and therefore the calculated Mach number are inaccurate, affecting the calibrated angle-of-attack data [36]. Although the correlation coefficient between these two data is ($p = 0.5067$), the angle-of-attack data was not included in the airspeed sensor fault analysis. In this way, data related to the airspeed and their correlation coefficients are given in Table 3.

2.3 Training by adaptive neural fuzzy inference system

In this study, ANFIS and ANN were used in fault detection and system reconstruction. The advantage of using relevant methods when compared to model-based ones in the literature such as Kalman filter and Luenberger observer is that relevant methods are model-free and it has error tolerance. Therefore, this machine learning methods can easily be used for non-linear systems such as aircrafts without the obligation of having certain assumptions [37]. In addition, the proposed approach presents more preciseness, fast fault detection and reconstruction without increasing system complexity, computational power and cost and it is suitable fast real time operations. Normalization process was not carried out for this study. This can be useful in some case where all parameters must have the same positive scale. However, it causes outliers to be lost. Because of that, normalisation step was not preferred to use in this study. As a result of the comparison of ANFIS and ANN, it was observed that the ANN gives more accurate results for this study.

Adaptive neural fuzzy inference system produces a single output and uses the weighted average defuzzification method. Output membership functions are all the same type of constant or linear function. The items that need to be determined in order to use the application are the number of linguistic

https://doi.org/10.1017/aer.2021.118 Published online by Cambridge University Press

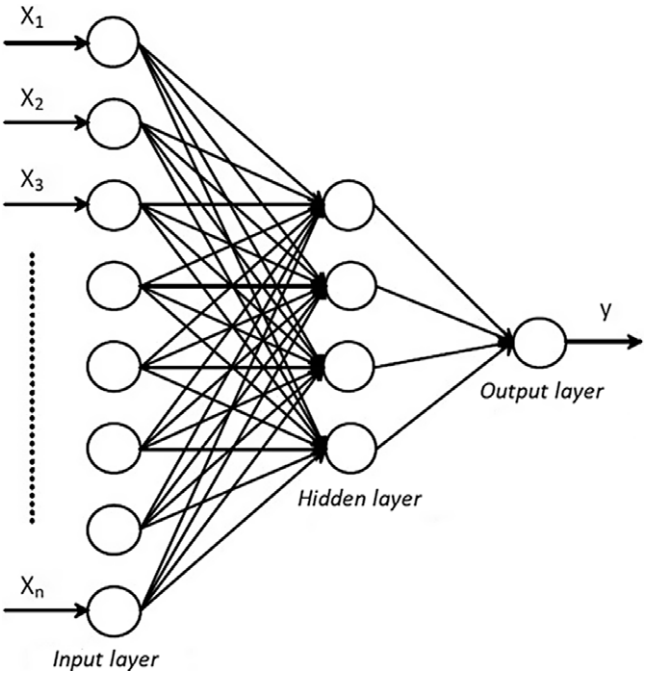

Figure 2. *Neural network structure.*

variables, membership function type, degree of fuzzy inference, optimisation method, error tolerance and epoch number [38]. Three membership functions are defined for each input to train ANFIS. Each type of membership function has been tested (triangular, trapezoidal, generalised bell-shaped, gaussian, pi-shaped, sigmoidal). The output membership function is taken as constant in the fuzzy inference section. Optimiation method selected as hybrid. Error tolerance is set to zero. The epoch number was taken as 3 (usually gives the optimal result in the 2nd epoch) for ANFIS training. Training and test data has been chosen randomly (%70-%30). The most related data have been chosen, as too many rules can occur. The most related data according to the correlation coefficients for angle-of-attack; static pressure, calibrated airspeed, pitch angle, engine N1 shaft speed. The relevant four values form the input of the ANFIS, while the angle-of-attack forms the output data. RMSE was calculated for each membership function, and minimum RMSE (0.914030) was obtained for the triangular membership function. The most related data according to the correlation coefficients for airspeed; static pressure, pitch angle, static air temperature, engine N1 shaft speed. The relevant four values form the input of the ANFIS, while the airspeed forms the output data. RMSE was calculated for each membership function, and minimum RMSE (4.832116) was obtained for the triangular membership function.

2.4 Training by artificial neural network

A neural network consists of an input layer, hidden layer, and an output layer. In this study, a feedforward multilayer perceptron was used. MATLAB Neural Network Toolbox was used for the operations. A neural network structure is given in Fig. 2.

Levenberg Marquardt *(trainlm)* was preferred for the training algorithm. Back propagation algorithm *(learngdm)* is used as learning algorithm, while Tan-Sigmoid Transfer Function *(tansig)* is used as activation function. In order to use Tan-Sigmoid Transfer Function, input values are first normalised between $(-1, 1)$ and consequently output values are obtained between $(-1, 1)$. Tan-Sigmoid Transfer Function is given in Equation (9) [38].

$$Tansig\ (n) = \frac{2}{(1 + e^{-2n})} - 1 \tag{9}$$

https://doi.org/10.1017/aer.2021.118 Published online by Cambridge University Press

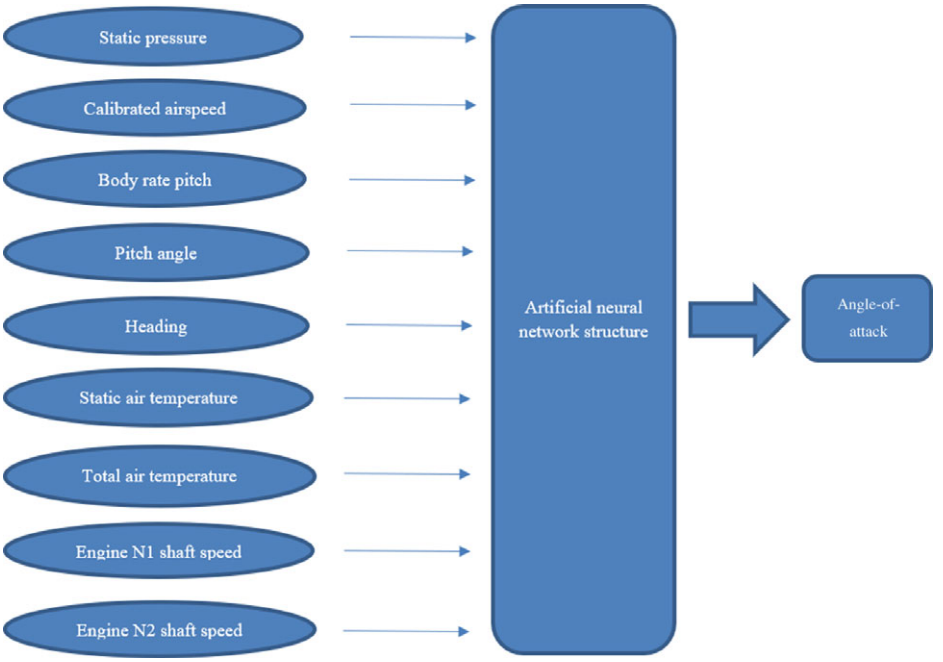

Figure 3. *The ANN structure for the angle-of-attack.*

The hidden layer number is taken as 1 for the algorithm to work faster. One of the most important parameters in training an artificial neural network is how many neurons are in the hidden layers. Since there are no definite rules in determining this situation, the appropriate number can be determined by gradually increasing starting from certain numbers. The total input output real data set which is collected from a commercial aircraft is (36,550) and the total input output dataset is randomly divided into training (25,585) and test set (10,965). The net output of the neural network is calculated using Equation (10) [38].

$$F\,(Net) = \frac{e^{Net} - e^{-Net}}{e^{Net} + e^{-Net}} \tag{10}$$

3.0 Simulation results

In order to compare ANFIS and ANN, first the ANN was trained and tested for **the most related data** for the angle-of-attack. The relevant four values form the input of the ANN, while the angle-of-attack forms the output data. The data estimation performance parameter RMSE of the ANN is 0.8780 for four neurons structure in the hidden layer and 0.8170 for eight neurons structure in the hidden layer. After that, analysis will be carried out based on **related data** for the angle-of-attack. Correlation analysis results of nine input data related to the angle-of-attack were found in section 2.2. In Fig. 3, the ANN structure created for nine related data of the angle-of-attack is given.

The numbers of 3, 9 and 18 neurons structure were examined for the related data with the angle-of-attack. The angle-of-attack regression curves for 18 neurons structure for training, validation and test of the network are shown in Fig. 4. The test data estimation performance parameters root mean squared error (RMSE) and coefficient of determination (R^2) are given in Table 4. The network that has the minimum RMSE and the maximum R^2 was accepted as the best model.

When examining the relevant values for the angle-of-attack, 18 neurons structure gives the best test result. In Fig. 5(a), the real and estimated angle-of-attack data are given for 18 neurons structure. As can be seen, the estimated angle-of-attack values displayed in orange match with the real angle-of-attack

https://doi.org/10.1017/aer.2021.118 Published online by Cambridge University Press

Table 4. RMSE and R^2 for estimation of the angle-of-attack

The hidden layer neuron	RMSE	$\mathbf{R^2}$
3	0.7702	0.872
9	0.5832	0.927
18	0.5127	0.943

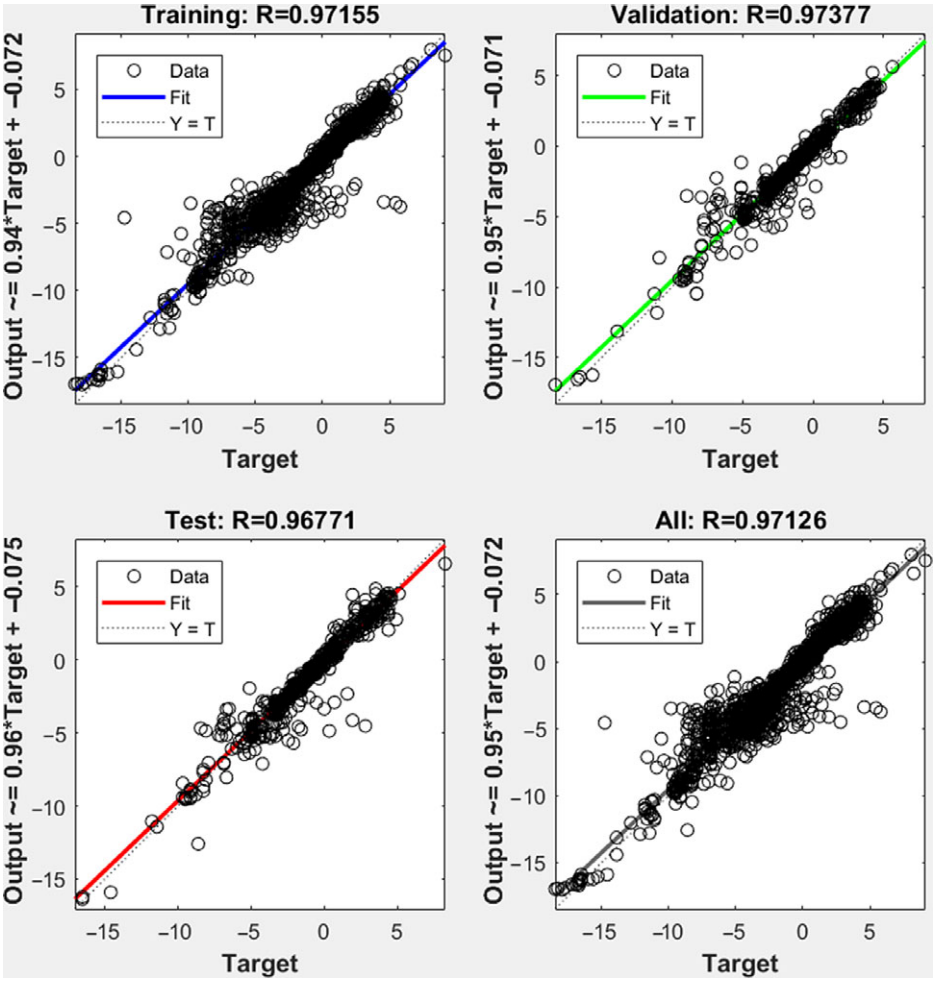

Figure 4. *The angle-of-attack regression curves for 18 neurons structure.*

values shown in blue throughout most of the flight. In Fig. 5(b), the absolute value of the difference *"|r(k)|"*, between the real angle-of-attack data without fault *"y(k)"* and the estimated angle-of-attack data *"ŷ(k)"* is given.

As mentioned in section 2.1, it is stated that there is no fault condition up to the threshold value of $\varepsilon_1 = 10$ degrees for the angle-of-attack data. It was subjected to an evaluation according to the relevant threshold value and although the system was tested according to non-fault data, it was observed that false alarm occurred at t = 10,621.s due to estimation error (the corresponding value is 10.1933).

If an examination is carried out for the airspeed; first, the ANN was trained and tested for **the most related data**. The relevant four values form the input of the ANN, while the airspeed forms the output data in training. The data estimation performance parameter RMSE of the ANN is 5.3644 for four

https://doi.org/10.1017/aer.2021.118 Published online by Cambridge University Press

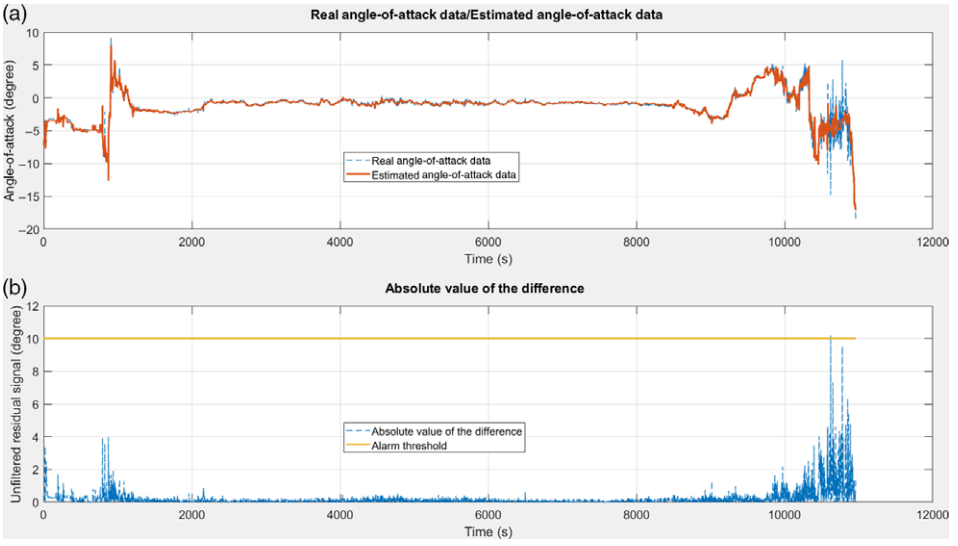

Figure 5. *The real and estimated angle-of-attack data and the absolute value of the difference.*

Figure 6. *The real and estimated airspeed data and the absolute value of the difference.*

neurons structure and 4.0871 for eight neurons structure. After that, analysis will be carried out based on **related data** for the airspeed. Correlation analysis results of seven input data related to the airspeed were found in section 2.2. The numbers of 3, 7 and 14 neurons structure were examined for the related data with the airspeed. When examining the relevant values for the airspeed, 14 neurons structure gives the best test result (RMSE = 1.1944). In Fig. 6(a), the real and estimated airspeed data are given for 14 neurons structure. As can be seen, the estimated airspeed values displayed in orange match with the real airspeed values shown in blue throughout most of the flight. In Fig. 6(b), the absolute value of the difference *"|r(k)|"*, between the real airspeed data without fault *"y(k)"* and the estimated airspeed data *"$\hat{y}(k)$"* is given.

As mentioned in section 2.1, it is stated that there is no fault condition up to the threshold value of $\varepsilon_1 = 4$ knots for the airspeed data. It was subjected to an evaluation according to the relevant threshold

https://doi.org/10.1017/aer.2021.118 Published online by Cambridge University Press

Table 5. *Comparison of analysis methods for the data estimation*

Sensor type	Analysis method	RMSE
Angle-of-attack	ANFIS triangular membership function	0.914030
	ANN 4 inputs and 8 neurons structure	0.8170
	ANN 9 inputs and 18 neurons structure	0.5127
Airspeed	ANFIS triangular membership function	4.832116
	ANN 4 inputs and 8 neurons structure	4.0871
	ANN 7 inputs and 14 neurons structure	1.1944

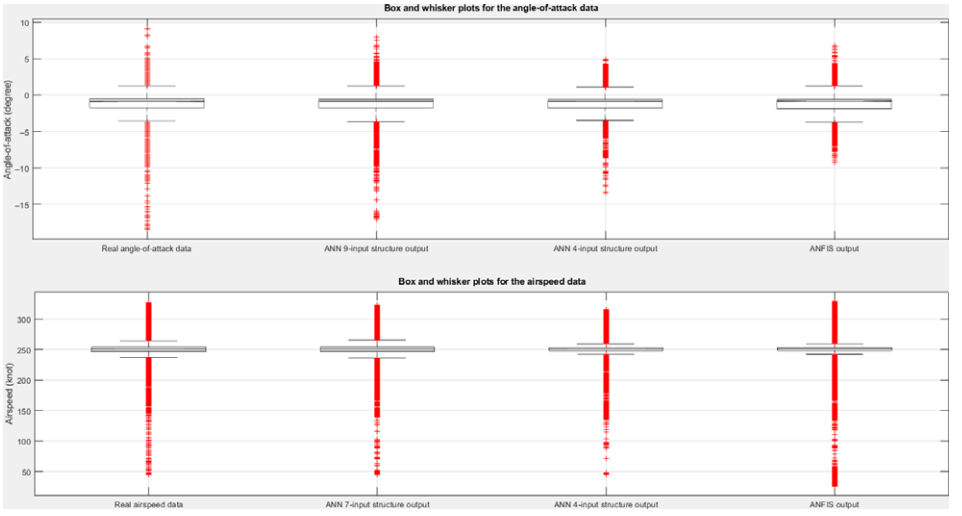

Figure 7. *Box and whisker plots for the data estimation.*

value and although the system was tested according to non-fault data, it was observed that false alarms occurred at 93 points due to estimation error. The minimum estimation error RMSE among the methods examined for the estimation of the angle-of-attack and airspeed test data are given in Table 5. In the next part of the study, firstly, each fault scenario will be modeled and the absolute values of the residual signals obtained here will be filtered through the *"gaussian filter"* for the angle-of-attack and the *"movmean filter",* for the airspeed and false alarm conditions will be eliminated and faults will be tried to be detected.

From those results, it is seen that the ANN gives more accurate results for this study. In Fig. 7, box and whisker plots are given for each method. A box plot provides a visualisation of summary statistics. In the evaluation carried out on the basis of the median values of the estimated sensor data and the bottom and top of the boxes, it was seen that the ANN estimates the real sensor data with higher accuracy. Therefore, instead of adding a new sensor, the estimated values that will be using for the fault detection and reconstruction according to the required values will be obtained from artificial neural networks.

4.0 Fault modeling, detection and system reconstruction

In this study, bias (positive or negative offset), oscillation, stuck at last sensor value, stuck at zero, NRZ (Non-Return to Zero), drift error (runaway error) and noise type (white noise, random noise) faults which may occur in the sensors according to real flight data have been examined. The flight phases where the faults occurred were modeled according to the climb after approximately t = 900.s, the cruise after approximately t = 2,500.s and the descent after approximately t = 8,500.s of the flight. Information on the faults modeled for the angle-of-attack sensor are given in Table 6.

https://doi.org/10.1017/aer.2021.118 Published online by Cambridge University Press

Table 6. *Faults modeled for the angle-of-attack sensor*

Fault type *{f(k)}*	**Flight phase**	**Fault amplitude (degree)**	**Fault time interval (s)** $\{t_1 \leq t \leq t_2\}$	**Fault detection time (s)**
Bias	Climb	10 degrees	$1{,}000 \leq t \leq 2000$	Instant
Oscillation	Climb	10 degrees amplitude cos wave with 10 hertz frequency	$2000 \leq t \leq 2{,}500$	1
NRZ	Cruise	10 degrees amplitude square wave with 10 hertz frequency	$2{,}500 \leq t \leq 3{,}500$	1
Drift	Cruise	3 t	$7{,}500 \leq t \leq 7{,}505$	Instant
Noise	Descent	Random noise	$9{,}000 \leq t \leq 9{,}500$	Instant

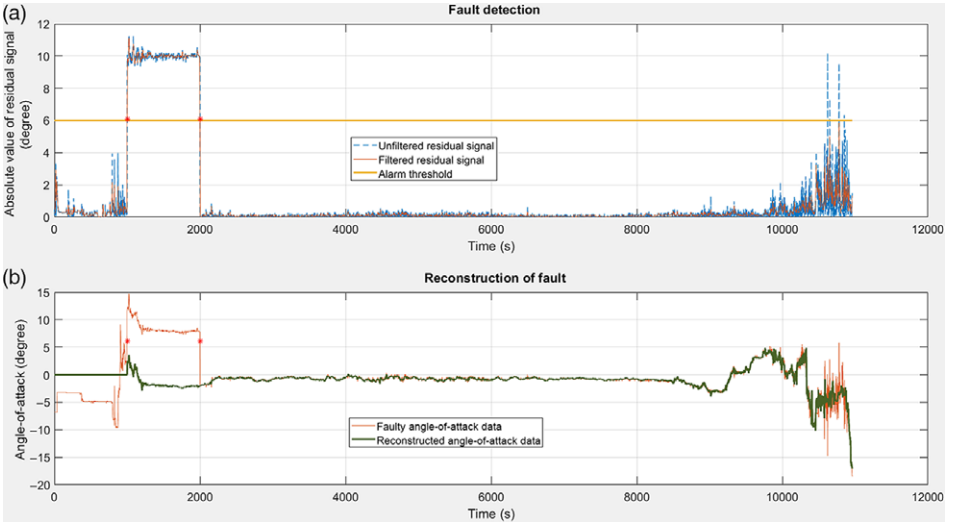

Figure 8. *Bias type fault detection and reconstruction for the angle-of-attack sensor.*

While the absolute values of the residual signals for bias, oscillation, NRZ, drift and noise type faults modeled according to Table 6 are given as unfiltered and filtered in Fig. 8(a), Fig. 9(a), Fig. 10(a), Fig. 11(a) and Fig. 12(a), the fault reconstructions by using the analytical redundant system are seen in Fig. 8(b), Fig. 9(b), Fig. 10(b), Fig. 11(b) and Fig. 12(b). The fault can be intervened instantaneously by transferring the estimated values *"$\hat{y}(k)$"* to the output, obtained by using ANN instead of the faulty values *"$Y(k)$"*. Here, after filtering the residual signal, a new threshold value is determined (ε_2=6 degrees) instead of the ε_1=10 degrees for the angle-of-attack. The threshold change could be seen in Fig. 8(a), Fig. 9(a), Fig. 10(a), Fig. 11(a) and Fig. 12(a). As shown in the Fig. 8, Bias type fault is generated at t = 1,000.s (the part where the orange-coloured filtered signal exceeds the threshold value of ε_2=6 degrees is t = 1,000.s, and this value is 6.0766). As shown in the Fig. 9, Oscillation type fault is generated at t = 2000.s (the part where the orange-coloured filtered signal exceeds the threshold value of ε_2=6 degrees is t = 2001.s and this value is 7.6545). As shown in the Fig. 10, NRZ type fault is generated at t = 2,500.s (the part where the orange-coloured filtered signal exceeds the threshold value of ε_2=6 degrees is t = 2,501.s and this value is 7.7283). As shown in the Fig. 11, Drift type fault is generated at t = 7,500.s (the part where the orange-coloured filtered signal exceeds the threshold value of ε_2=6 degrees is t = 7,500.s and this value is 6.2414). As shown in the Fig. 12, Noise type fault is generated at t = 9,000.s (the part where the orange-coloured filtered signal exceeds the threshold value of ε_2=6 degrees is t = 9,000.s and this value is 7.1447). Next, a fault analysis will be carried out for the airspeed sensor. Information on the faults modeled for the airspeed sensor are given in Table 7.

https://doi.org/10.1017/aer.2021.118 Published online by Cambridge University Press

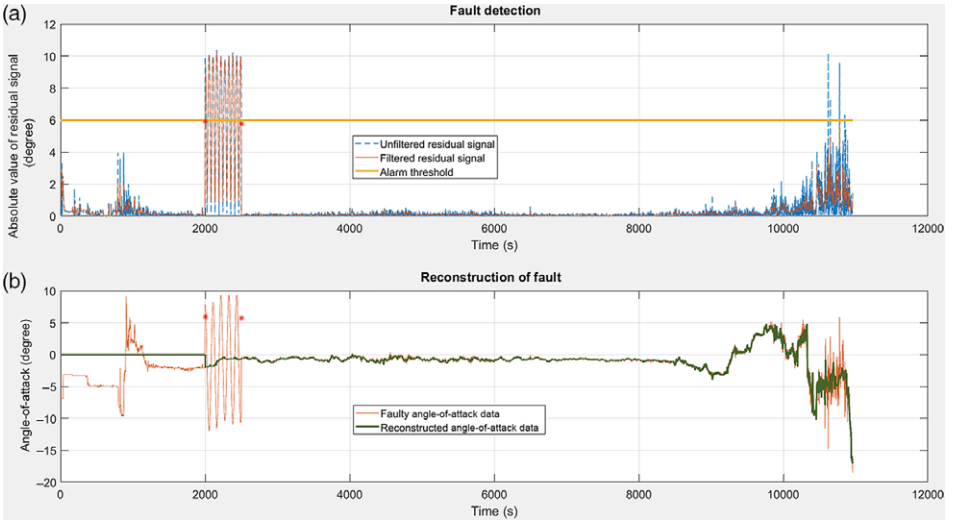

Figure 9. *Oscillation type fault detection and reconstruction for the angle-of-attack sensor.*

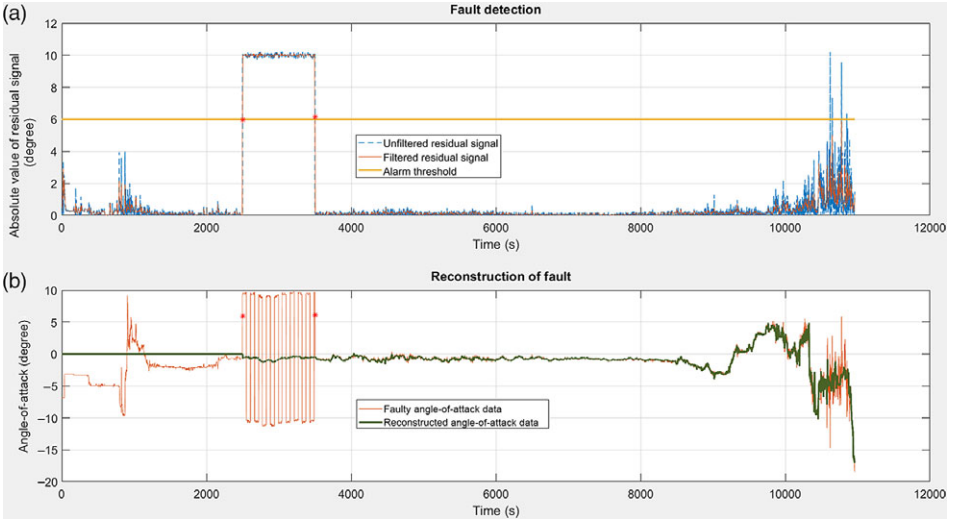

Figure 10. *NRZ type fault detection and reconstruction for the angle-of-attack sensor.*

While the absolute values of the residual signals for stuck at last sensor value and stuck at zero type faults modeled according to Table 7 are given as unfiltered and filtered in Fig. 13(a) and Fig. 14(a), the fault reconstructions by using the analytical redundant system are seen in Fig. 13(b) and Fig. 14(b). Here, after filtering the residual signal, a new threshold value is determined ($\varepsilon_2 = 3$ knots) instead of the $\varepsilon_1 = 4$ knots for the airspeed. The threshold change could be seen in Fig. 13(a) and Fig. 14(a). As shown in the Fig. 13, Stuck at last sensor value type fault is generated at t = 2000.s (the part where the orange-coloured filtered signal exceeds the threshold value of $\varepsilon_2 = 3$ knots is t = 2000.s and this value is 3.0228). As shown in the Fig. 14, Stuck at zero type fault is generated at t = 8,000.s (the part where the orange-coloured filtered signal exceeds the threshold value of $\varepsilon_2 = 3$ knots is t = 8,000.s and this value is 125.7958).

https://doi.org/10.1017/aer.2021.118 Published online by Cambridge University Press

Table 7. *Faults modeled for the airspeed sensor*

Fault type ***{f(k)}***	**Flight phase**	**Fault amplitude (knot)**	**Fault time interval (s)** $\{t_1 \leq t \leq t_2\}$	**Fault detection time (s)**
Bias	Climb	4 knots	$1{,}000 \leq t \leq 1{,}500$	Instant
Oscillation	Climb	4 knots amplitude cos wave with 10 hertz frequency	$1{,}000 \leq t \leq 2000$	Instant
Stuck at last sensor value	Climb	286 knots	2000.s	Instant
Stuck at zero	Cruise	Zero	8,000.s	Instant
NRZ	Descent	4 knots amplitude square wave with 10 hertz frequency	$8{,}500 \leq t \leq 9{,}000$	Instant
Noise	Descent	Random noise	$9{,}000 \leq t \leq 9{,}500$	Instant

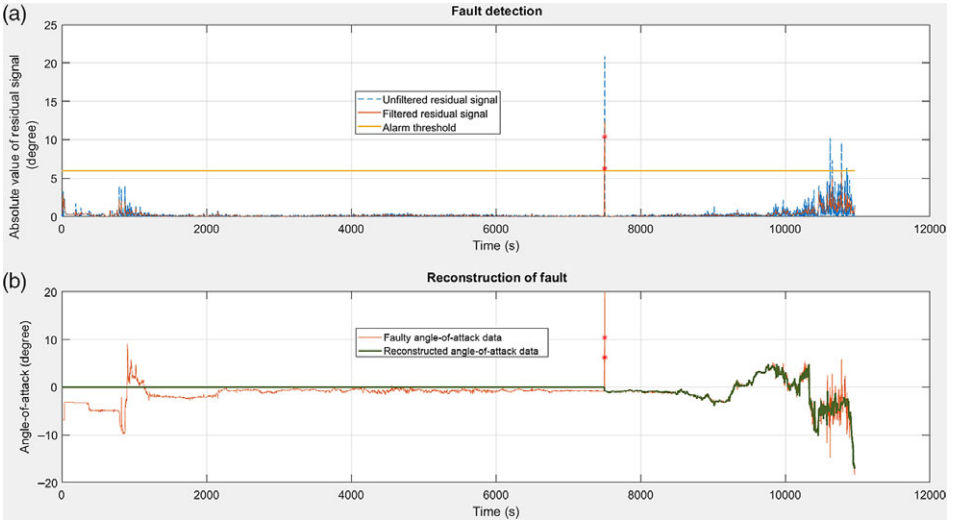

Figure 11. *Drift type fault detection and reconstruction for the angle-of-attack sensor.*

Conclusions

In this study, fault detection and reconstruction were carried out by using Adaptive Neural Fuzzy Inference System (ANFIS) and Artificial Neural Networks (ANN) by estimating the required values of the angle-of-attack and airspeed data in all flight phases. Correlation analysis was performed to select the data related to the angle-of-attack and airspeed. The residual signals were filtered to eliminate the false alarm conditions. The absolute values of the residual signals obtained were evaluated according to a certain threshold value. The fault detection and reconstruction were carried out 0–1 s for angle-of-attack sensor and instantaneously for airspeed sensor. The point to note here is that the data used for the fault reconstruction are not obtained from any redundant element and are estimated from other data. In other words, a visual sensor structure is created with the help of the analytical relations. In addition, the proposed scheme provides an alternative method for calculating angle-of-attack and airspeed data. In this study, a safer fault detection and reconstruction system was created for angle-of-attack and airspeed sensors, with an annual fuel saving of approximately 20 tons, gaining distance of 8,000 km and CO_2 emission less than 63.2 tons, without relying on hardware redundancy and pitot-static measurements. Instead of a system like BUSS and SAS used in commercial aircrafts, the designed system contains

https://doi.org/10.1017/aer.2021.118 Published online by Cambridge University Press

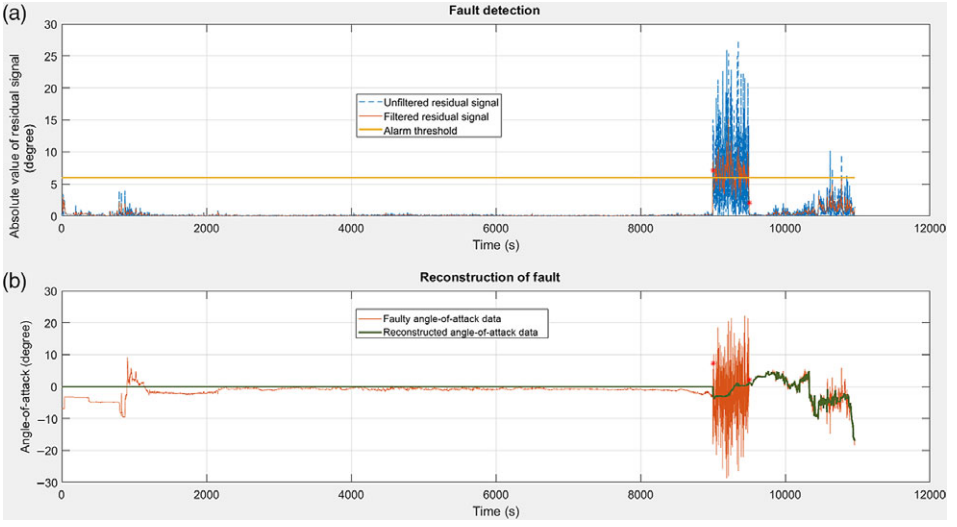

Figure 12. *Noise type fault detection and reconstruction for the angle-of-attack sensor.*

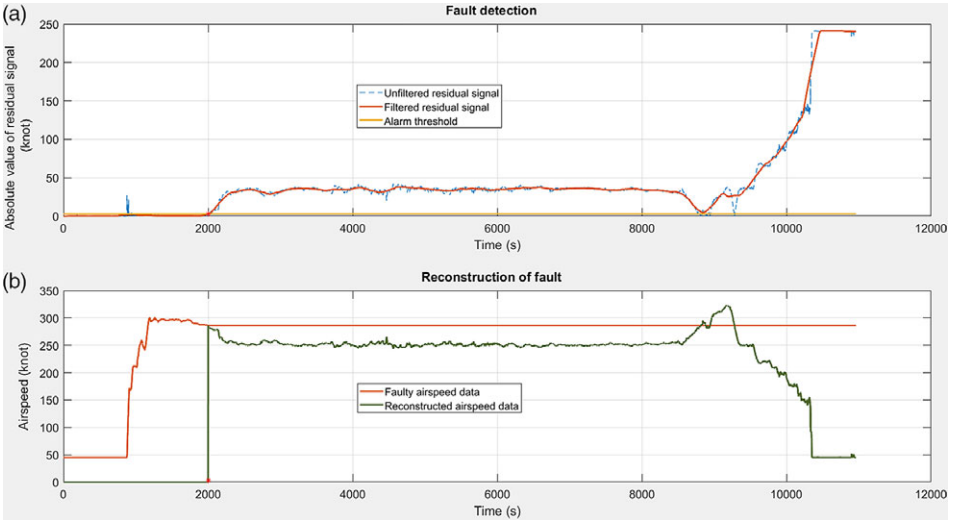

Figure 13. *Stuck at last sensor value type fault detection and reconstruction for the airspeed sensor.*

more parameters for estimation and the higher number of input parameters and hidden layer neurons give more accurate results as it is stated in further works of some studies and in our study. In order to prevent accidents in aircrafts, a system that works in real time and accurately can be installed on aircrafts. Since future works will be on fault detection and reconstruction using online training, methods such as deep learning are not preferred because they are not faster than the classical Artificial Neural Network algorithms. Also, the accuracy of the system could be measured with real flight data after the relevant aircraft have been modeled using flight dynamics. The desired aircraft could be modeled using aerodynamic flight coefficients. When modeling aircraft, aircraft dynamics, validated models of the flight environment and pilot behaviour will be included in the relevant aircraft system. After the modeling of the desired aircraft, analysis such as fault detection, diagnosis and estimation for the relevant aircraft are examined in the desired flight conditions.

https://doi.org/10.1017/aer.2021.118 Published online by Cambridge University Press

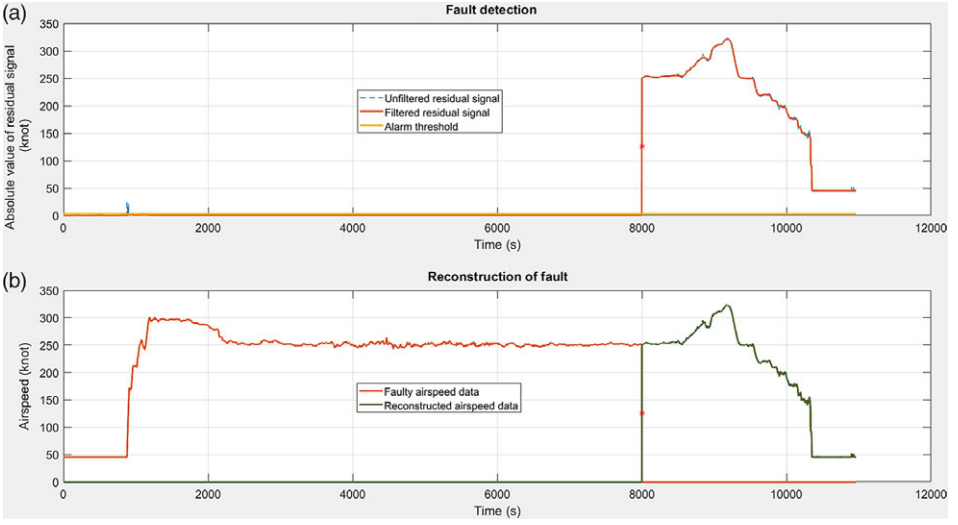

Figure 14. *Stuck at zero type fault detection and reconstruction for the airspeed sensor.*

Acknowledgment. This study was supported by Eskisehir Technical University Scientific Research Projects Commission under the grant no: 20DRP050.

References

[1] Alvarez, O.H., Zea, L.B.G., Bil, C., Napolitano, M. and Fravolini, M.L. Review of methodologies for aircraft sensors fault detection and correction, *International Symposium on Space Flight Dynamics, Melbourne-Australia*, 2019, pp 259–264.

[2] Ossmann, D. and Joos, H.D. Enhanced detection and isolation of angle of attack sensor faults, *AIAA Guidance, Navigation and Control Conference*, San Diego, California-USA, 2016, pp 1–16.

[3] Taimoor, M. and Aijun, L. Neural-sliding mode approach-based adaptive estimation, isolation and tolerance of aircraft sensor fault, *Aircr. Eng. Aerosp. Technol.*, 2019, **92**, (2), pp 237–255.

[4] Yildirim Dalkiran, F. and Toraman, M. Predicting thrust of aircraft using artificial neural networks, *Aircr. Eng. Aerosp. Technol.*, 2020, **92**, (2), pp 237–255.

[5] Verma H.O. and Peyada N.K. Parameter estimation of aircraft using extreme learning machine and Gauss-Newton algorithm, *Aeronaut. J.*, 2020, **124**, (1272), pp 271–295.

[6] Can, E. Application of Adaptive Neuro-Fuzzy Logic Method of Noised Electrical Signals for Correction, *Tecciencia*, 2020, **15**, (28), pp 1–13.

[7] Hardalaç, F., Aydın, M., Kutbay, U., Ayturan, K., Akyel, A., Çağlar, A., Hai, B. and Mert, F. Classification of neonatal jaundice in mobile application with noninvasive image processing methods, *Turk. J. Electr. Eng. Comput. Sci.*, 2021, **29**, pp 2116–2126.

[8] Verma, H.O. and Peyada, N.K. Estimation of aerodynamic parameters near stall using maximum likelihood and extreme learning machine-based methods, *Aeronaut. J.*, 2021, **125**, (1285), pp 489–509.

[9] Atasoy, V.E., Suzer, A.E. and Ekici, S.A. Comparative Analysis of Exhaust Gas Temperature Based on Machine Learning Models for Aviation Applications, *J. Energy Resour. Technol.*, 2021, **144**, (8): 082101.

[10] Popowski, S. and Dabrowski, W. Measurement and estimation of the angle of attack and the angle of sideslip, *Vilnius Gedim. Tech. Univ. Press,* 2015, **19**, (1), pp 19–24.

[11] Milward, T.O., Bromfield, M., Horri, N., Ali, R. and Scott, S. Multipoint Angle of Attack Sensing for Avoidance of Loss of Control in Flight, *AIAA SCITECH*, San Diego, California-USA, 2019, pp 1–16.

[12] Joos, H.D. and Ossmann, D. Enhancing flight control in case of total angle of attack sensor loss, *3rd International Conference on Control and Fault Tolerant Systems*, Barcelona, Spain, 2016, pp 783–789.

[13] Ossmann, D. and Joos, H.D. Combining sensor monitoring and fault tolerant control to maintain flight control system functionalities, *20th IFAC Symposium on Automatic Control in Aerospace*, San Diego, California-USA, 2016, pp 46–51.

[14] Mako, S., Pilat, M., Svab, P., Kozuba, J. and Cicvakova, M. Evaluation of MCAS system, *Acta Avionica J.*, 2020, **40**, (1), pp 21–28.

[15] Dia. Gas turbine engines, *Aviat. Week*, 2008, **168**, (4), pp 128–143.

[16] Orhan, I., Kapanoğlu, M. and Karakoç, T.H. Concurrent aircraft routing and maintenance scheduling using goal programming, *J. Fac. Eng. Archit. Gazi Univ.*, 2012, **27**, (1), pp 11–26.

[17] Roberson, B. Fuel conservation strategies, *Aero*, 2007, **2**, (10), pp 26–28.

https://doi.org/10.1017/aer.2021.118 Published online by Cambridge University Press

[18] Turgut, E.T., Usanmaz, O. and Cavcar, M. The effect of flight distance on fuel mileage and CO2 per passenger kilometer, *Int. J. Sustain. Transp.*, 2019, **13**, (3), pp 224–234.
[19] Eykeren, L.V. and Chu, Q.P. Sensor fault detection and isolation for aircraft control systems by kinematic relations, *Control Eng. Pract.*, 2014, **31**, pp 200–210.
[20] Purvis, A., Morris, B. and Mcwilliam, R. FlightGear as a tool for real time fault injection, detection and self repair, 4. *International Conference on Through life Engineering Services*, 2015, Cranfield-UK, pp 283–288.
[21] Singh, S. and Murthy, T. Simulation of sensor failure accommodation in flight control system of transport aircraft : a modular approach, *World J. Model. Simul.*, 2015, **11**, (1), pp 55–68.
[22] Zolghadri, A., Cieslak, J., Efimov, D., Henry, D., Philippe, G., Dayre, R., Gheorghe, A. and Berre, H.L. Signal and model-based fault detection for aircraft systems, 9. *IFAC Symposium on Fault Detection, Supervision and Safety for Technical Processes*, 2015, Paris-France, pp 1096–1101.
[23] Sercekman, O. and Kutay, A.T. A model based approach for sensor fault detection in civil aircraft control surface, *IEEE/ION Position, Location and Navigation Symposium*, Monterey, CA-USA, 2018, pp 715–729.
[24] Lijia, C., Yu, T. and Guo, Z. Adaptive observer-based fault detection and active tolerant control for unmanned aerial vehicles attitude system, 5. *IFAC Symposium on Telematics Applications, Chengdu-China*, 2019, pp 47–52.
[25] He, Q., Zhang, W., Lu, P. and Liu, J. Performance comparison of representative model based fault reconstruction algorithms for aircraft sensor fault detection and diagnosis, *Aerosp. Sci. Technol.,* 2020, **98**, (105649).
[26] Sun, K. and Gebre, E.D. A fault detection and isolation design for a dual pitot tube air data system, *IEEE/ION Position, Location and Navigation Symposium*, Portland, OR-USA, 2020, pp 62–73.
[27] Turkmen, I. An alternative neural airspeed computation method for aircrafts, *Aircr. Eng. Aerosp. Technol.*, 2018, **90**, (2), pp 368–378.
[28] Fravolini, M.L., Napolitano, M.R., Core, G. and Papa, U. Experimental interval models for the robust fault detection of aircraft air data sensors, *Control Eng. Pract.*, 2018, **78**, pp 196–212.
[29] Lu, P., Kampen, E.J.V., Visser, C. and Chu, Q. Air data sensor fault detection and diagnosis in the presence of atmospheric turbulence: theory and experimental validation with real flight data, *IEEE Trans. Control Syst. Technol.*, 2020, pp 1–9.
[30] Fekih, A. Fault diagnosis and fault tolerant control design for aerospace systems: A bibliographical review, *American Control Conference*, Portland, OR-USA, 2014, pp 1286–1291.
[31] Samy, I., Postlethwaite, I. and Gu, D. Survey and application of sensor fault detection and isolation schemes, *Control Eng. Pract.*, 2011, **19**, (7), pp 658–674.
[32] Castaldi, P., Mimmo, N. and Simani, S. Avionic air data sensors fault detection and isolation by means of singular perturbation and geometric approach, *Sensors*, 2017, **17**, (2202), pp 1–19.
[33] Oliveira, L.R.M. The dramatic effects of pitot static system blockages and failures, 2013, available at: http://www.luizmonteiro.com/DocumentsPDF/The_Dramatic_Effects_of_Pitot_Static_Blockages.pdf (accessed 24 June 2021)
[34] Freeman, P., Seiler, P. and Balas, G.J. Air data system fault modeling and detection, *Control Eng. Pract.*, 2013, **21**, (10), pp 1290–1301.
[35] Duda, R.O., Hart, P.E. and Stork, D.G. *Pattern classification,* John Wiley & Sons, 2000, New York, USA.
[36] Cashman, J.E., Kelly, B.D. and Nield, B.N. Operational use of angle of attack on modern commercial jet airplanes, *Aero*, 2000, **12**, pp 12–21.
[37] Singh, S. and Vasudeviah, R.M.T. Neural network based sensor fault detection for flight control systems, *Int. J. Comput. Applications*, 2012, **59**, (13), pp 1–8.
[38] Rencber, O.F. *Multiple logistic regression in classification problems, comparison of ANN and ANFIS methods: Application on human development index,* Gazi Press, 2018, Ankara, Turkey.

Cite this article: Kilic U. and Unal G. (2022). Sensor fault detection and reconstruction system for commercial aircrafts. *The Aeronautical Journal*, **126**, 889–905. https://doi.org/10.1017/aer.2021.118
https://doi.org/10.1017/aer.2021.118 Published online by Cambridge University Press